Nano Energy 67 (2020) 104266

Contents lists available at ScienceDirect

Nano Energy

journal homepage: http://www.elsevier.com/locate/nanoen

Battery-free short-range self-powered wireless sensor network (SS-WSN) using TENG based direct sensory transmission (TDST) mechanism

Feng Wen [a,b,c,d,1], Hao Wang [a,b,c,d,1], Tianyiyi He [a,b,c,d,1], Qiongfeng Shi [a,b,c,d], Zhongda Sun [a,b,c,d], Minglu Zhu [a,b,c,d], Zixuan Zhang [a,b,c,d], Zhiguang Cao [e], Yanbing Dai [e], Ting Zhang [e,**], Chengkuo Lee [a,b,c,d,*]

[a] Department of Electrical & Computer Engineering, National University of Singapore, 4 Engineering Drive 3, 117576, Singapore
[b] National University of Singapore Suzhou Research Institute (NUSRI), Suzhou Industrial Park, Suzhou, 215123, China
[c] Center for Intelligent Sensors and MEMS, National University of Singapore, 4 Engineering Drive 3, 117576, Singapore
[d] Hybrid Integrated Flexible Electronic Systems (HIFES), 5 Engineering Drive 1, 117608, Singapore
[e] I-Lab Suzhou Institute of Nano-Tech and Nano-Bionics, Chinese Academy of Sciences (CAS), Suzhou, 215123, China

ARTICLE INFO

Keywords:
Wireless sensor network
Switch
Textile TENG
Force sensing
2D/3D control

ABSTRACT

Wireless Sensor Networks (WSNs) bring the basis that the development of the Internet of Things (IoTs) relies on. However, external power requirement restricts the widespread applications of WSNs. Triboelectric nanogenerator (TENG) has been a promising candidate for energy harvesting and self-powered sensing, but most of the reported TENG-based WSNs need to store energy in a capacitor first and then power the wireless modules without a continuous sensing capability simultaneously. In this work, a battery-free short-range self-powered wireless sensor network (SS-WSN) is proposed by using TENG-based direct sensory transmission (TDST). By leveraging a mechanical switch or diode-switch combination, enhanced output and boosted frequency of TENG signal have been achieved by instantaneous discharging in a short period, initiating the potential for direct signal transmission without additional wireless modules and external power suppliers. Different from others' works, the stable resonant frequency is used to realize the force-sensing function with high sensitivity (434.7 $Hz.N^{-1}$), in which case a wireless real-time electronic scale is demonstrated. Additionally, by varying the connections of the textile TENGs or the capacitance of an external capacitor for distinguishable resonant frequencies generation, the multiple-freedom-degree 2D toy car control, and 3D VR drone control are demonstrated with a single coil.

1. Introduction

Nowadays, Wireless Sensor Networks (WSNs) have attracted lots of attention from researchers in a wide variety of areas due to their ubiquitous nature and their tremendous development in the Internet of Things (IoT) [1–5]. IoT, which enables the wireless connection and controlling of devices through the internet, has been used in diversified applications for remote monitoring and sensing, such as environmental monitoring [6,7], smart home [8,9], and healthcare [10–14]. With the rapid development of IoTs, wearable electronics, which shape the human lifestyle, are in a great demand for the applications of human-machine interfaces (HMIs) [15–22], control [23,24], communication [25] and wireless networks [1,26–29]. Due to its unique characteristics, such as light-weight, soft, permeable and conformable, the cost-effective textile has become a promising candidate for wearable sensors in IoT networks [30–33]. However, the large power consumption for long-term connectivity, especially with the increasing number of sensors becomes the major bottleneck of WSN technologies [34]. To overcome this issue, different kinds of energy harvesting techniques, which scavenge various forms of energy from the ambient environment, are explored extensively in recent years, including the solar energy [35], kinetic energy [36], thermal energy [37], and the radio frequency (RF) energy [38]. Nevertheless, most of the reported energy harvesting techniques for wireless sensing could only fulfil the function of battery life extension rather than eliminating the usage of power supply, where the scavenged energy is stored into a capacitor or battery for later use.

* Corresponding author. Department of Electrical & Computer Engineering, National University of Singapore, 4 Engineering Drive 3, 117576, Singapore.
** Corresponding author.
E-mail addresses: tzhang2009@sinano.ac.cn (T. Zhang), elelc@nus.edu.sg (C. Lee).
[1] These authors contributed equally.

https://doi.org/10.1016/j.nanoen.2019.104266
Received 22 September 2019; Received in revised form 19 October 2019; Accepted 2 November 2019
Available online 7 November 2019

Therefore, it is desirable to develop the fully self-powered wireless sensors for IoT applications that can largely reduce the overall power consumption of the WSN system. According to the system architecture of IoT technology, massive sensory information from these distributed sensors usually flows into an adjacent communication node which is responsible for long-distance data transmission [39]. Thus, a short-range sensor data transmission using battery-free technology is rather desirable in most of the IoT applications.

Due to the ubiquitous kinetic energy in our daily life, energy harvesters based on the mechanisms of piezoelectric [40–45], electromagnetic [46–48], and triboelectric [49–55] emerge to scavenge waste energy from vibrations, pressure, and stress-strain. Among them, the triboelectric nanogenerator (TENG) is obtaining more and more interest among diversified research areas benefiting from its advantages of various choices of materials, easy fabrication, simple working mechanism, portable, and low-cost. TENGs have demonstrated the diversified sensing applications, such as force/pressure sensing [56–59], strain sensing [60,61], vibration sensing [12,62–64], acoustic sensing [65], and chemical sensing [66–68] by means of self-powered sensing mechanism, which refers to that the sensing signal is generated by the external mechanical stimuli without any other power supply in this signal generation process. However, most of the TENG sensors still need wires as the connection to the readout circuit which requires a stable external power supply for enabling the proper function. To wirelessly transmit the TENG output, the current technology mainly adopts a discrete wireless module powered by an external source in the signal transmission process [69]. In this regard, a battery-free wireless TENG sensor remains a key challenge. On the other hand, various TENG-based sensing systems are reported for diversified sensing applications such as humidity sensing [70,71], temperature sensing [72], vibration sensing [28], location sensing [73], and traffic volume sensing [74]. However, the TENG in these systems only functions as a power source for converting different forms of mechanical energy into electrical energy, which will then be stored into a capacitor or battery to power the distributed sensors and wireless transmission modules. In this case, non-negligible charging time is inevitable, thus the sensing systems can only send out the monitoring signals discontinuously and it highly depends on the occasions of external mechanical sources such as vibration or pressure, which in most cases are irrelevant to the sensing parameters such as temperature or humidity.

Direct wireless transmission of the TENG signal has been envisioned over a long period but has not been realized until recent time due to the low-frequency characteristic of the TENGs. Lately, the integration of diversified mechanical switches with the TENGs to realize an instantaneous discharging has been reported as an effective method to boost up the frequency of the triboelectric output significantly [75–82]. With the aid of the deliberately designed switch as part of the TENG structure, a non-contact signal reception of the TENG output has been successfully demonstrated through a simple inductive coupling. However, the wireless TENG array with switch integration faces the challenges of simultaneous alignment of multiple pairs of coils and the incapacity to respond to the capacitance variation of the TENG device itself. Furthermore, the multiple coils could cause an increase in the complexity of the system design [83]. Besides, the wireless sensing majorly comes from the amplitude of the received resonant signal which is largely unstable under the ambient environment [71].

Herein, we report a battery-free short-range self-powered wireless network (SS-WSN) using the TENG-based direct sensory transmission (TDST) mechanism. With the aid of external switch, an instantaneous discharging can be achieved at any time the switch is closed, which has successfully boosted up the frequency of the TENG output. The direct TENG signal transmission now becomes feasible by simply connecting the TENG to a coil with a 1 m transmission range due to the boosted frequency. A narrow-gap textile-based TENG is developed as the individual pixel in the proposed SS-WSN, and its device structure is illustrated in the inset of Fig. 1(b). Differentiated from the previous work where the TENG signal amplitude is characterized as the sensing parameter, here we use the stable resonant frequency of the oscillating TENG output as the force calibration reference, which has solved the long-standing challenge of the TENG amplitude's susceptibility to humidity variations. Furthermore, a highly sensitive (434.7 $Hz.N^{-1}$) and large-range force sensing are achieved, in which case a wireless real-time electronic scale is demonstrated. Additionally, by alternating the connection of textile TENG and adjusting the external capacitor to generate distinguishable resonant frequency, the multiple-freedom-degree 2D toy car control and 3D VR drone control are demonstrated by using one pair of coils. The minimalist design achieved by single-pair coils is desirable to ease the WSN system construction. Looking forward, this frequency shift wireless sensing and controlling technology enabled by the TENG-based direct sensory transmission renders an effective approach towards an SS-WSN for the diversified IoT applications as shown in Fig. 1(a).

2. Methods to achieve frequency boost up by instantaneous discharging

Up to now, various TENGs, integrated with delicately designed mechanical switches for output enhancing and signal frequency boost up by instantaneous discharging, have been well investigated [75–82]. There are three universal approaches to realize frequency boost up with the traditional TENG for comparison purposes, as shown in Fig. 2(a–d). For the characteristics of the textile TENGs hereafter, if not mentioned specifically, each of them contains four pieces stacked together to ensure a large output for later wireless transmission. For traditional TENG, a TENG device is directly connected to a resistor (10 MΩ) as shown in the inset of Fig. 2(a). The charge transfer processes between two electrodes happen gradually during the contacting and separating processes if there is no switch. It has negative attributes such as large pulse width (166.2 ms and 406.1 ms for positive and negative half cycle, respectively), resulting in small output as shown in Fig. 2(a). The first approach, where the instantaneous discharging happens at positive cycle, is defined as "forward diode" that refers to the positive layer and negative layer connected to the corresponding polarities of a diode. A switch is connected to the diode in parallel, as shown in the inset of Fig. 2(b). When pressing the textile TENG, the negative charges will flow from the positive electrode of TENG, pass through the diode, flow to the TENG negative side and accumulate there since the releasing cycle cannot drive the accumulated charges to flow back to positive electrode because of cut-off diode until the switch is on. The positive instantaneous output (for press) is boosted around 2 times while negative output keeps the same with traditional TENG and the pulse width decreases from 166.2 ms to 39.3 ms as shown in Fig. 2(b). This instantaneous discharging process is similar with the discharging of a charged capacitor. Hence, the voltage profile would follow the shape of the typical discharging curve of a conventional capacitor, which is only affected by the equivalent capacitance of TENG, the number of charges, and the contact area of the two layers. The absolute value maximum positive voltage V^{+}_{max} can be expressed by Ref. [75].

$$V^{+}_{max} = \frac{\sigma A}{C_{press}} \tag{1}$$

Where σ is the triboelectric charge density of press, A is the contact area of two triboelectric layers, C_{press} is the capacitance when the textile TENG is pressed. The second approach is "reversed diode" that refers to two triboelectrification layers connected to converted polarities of diode with a parallel connected switch. Similarly, the negative instantaneous discharging for frequency boost up purpose is obtained by this approach. Fig. 2(c) indicates that the negative instantaneous output (for release) can be increased around 10 times but positive output remains the same as the traditional TENG, and pulse width is reduced from 406.1 ms to 31.7 ms due to the accumulated charges releasing in a short period. The

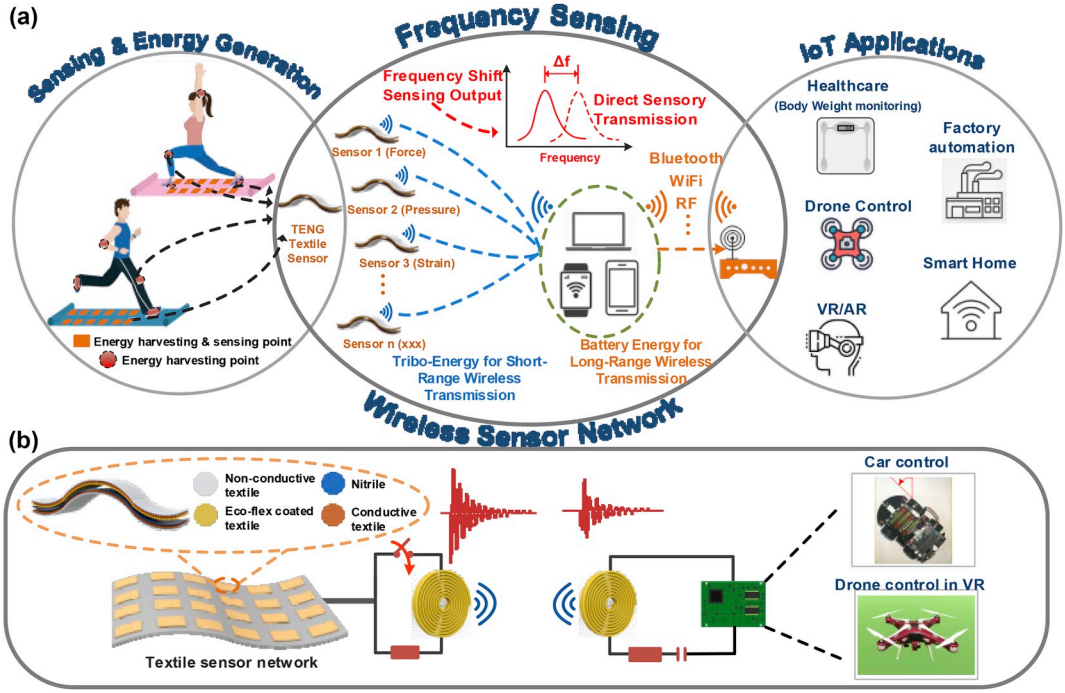

Fig. 1. **(a)** Illustration of the wireless TENG sensor network for diversified applications based on frequency shift. **(b)** The wireless TENG system for car control and drone control in VR based on RLC circuit.

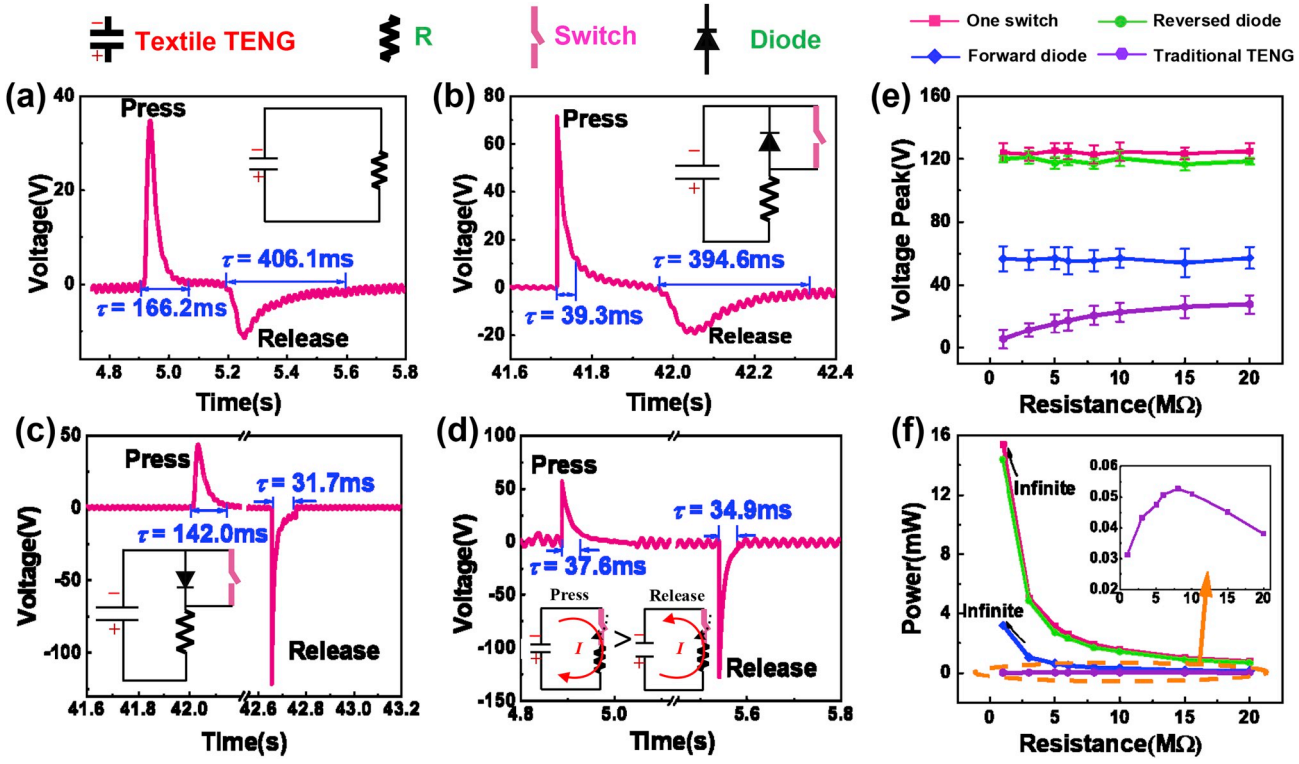

Fig. 2. The methods to achieve instantaneous discharging. **(a)** Traditional TENG. **(b)** Forward diode. **(c)** Reversed diode. **(d)** one switch. **(e)** The dependence of voltage peak on load resistance under 4 circuit conditions. **(f)** The power curves under 4 circuit conditions. The inset is the power curve of the traditional TENG.

absolute value of negative voltage V_{max}^{-} can also be express by

$$V_{max}^{-} = \frac{\sigma' A}{C_{release}} \tag{2}$$

Where σ' is the triboelectric charge density of release, $C_{release}$ is the capacitance when the narrow-gap TENG is released. By comparison, the increase of negative output for release in Fig. 2(c) is much more (10 times) than that of positive output for press (2 times) in Fig. 2(b). Theoretically, here the output for press is subject to the loading speed of mechanical stimuli such as force. The output dependence on speed of

pressing is shown in Fig. S1. It can be observed that the peak voltage gradually increases with the pressing speed. While the output for release is relevant to the soft characteristic of textile TENG and mainly determined by the natural and gradual separation process of two soft triboelectrification layers (i.e. soft nitrile and Ecoflex). During releasing, the separation speed of two layers is much slower than that of contact even external pressing and releasing speed are roughly equal. Therefore, larger pulse width and lower voltage peak are observed in release case while press case experiences smaller pulse width and higher peak value (Fig. 2(a)). By leveraging the mechanical switch or switch-diode combination, the enhanced output is achieved by instantaneous discharging, where the output for press and release increase by 2 times and 10 times, respectively. In other words, the voltage enhancement of press is not as obvious as release. It can be explained that since press has a higher output and a shorter pulse width than release due to the relatively high speed of contact, the enhancement of output is relatively less evident

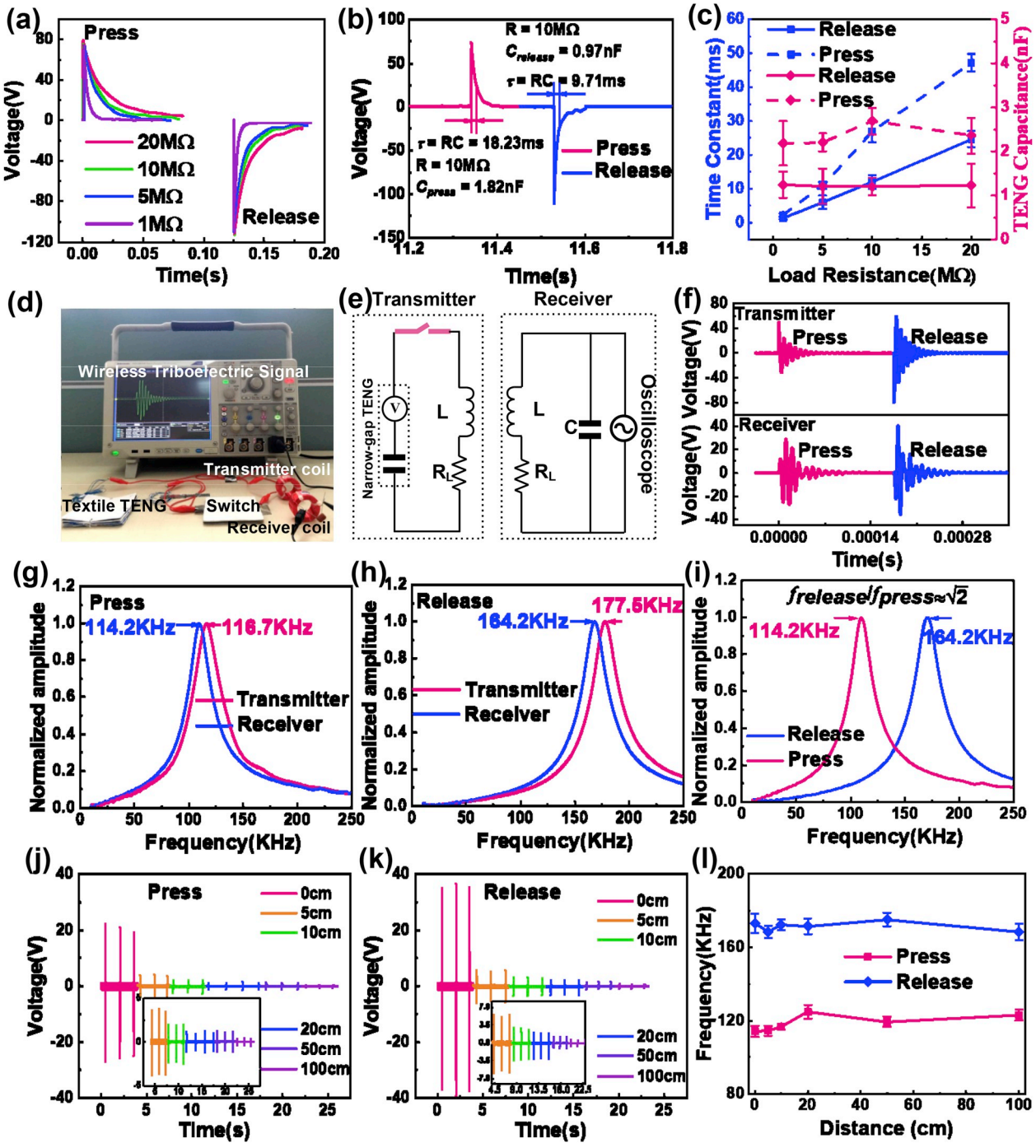

Fig. 3. The characterization of wireless textile TENG. **(a)** The instantaneous output under external load resistances 1 MΩ, 5 MΩ, 10 MΩ and 20 MΩ. **(b)** The detailed calculation of C_{press} and $C_{release}$. **(c)** The dependence of time constant and TENG capacitance on external load resistances under press and release conditions. **(d)** The set-up of wireless transmission. **(e)** The equivalent wireless transmission circuit based on single switch. **(f)** The signals of transmitter and receiver ($L = 1$ mH). **(g)** The frequency spectrums of press from transmitter and receiver. **(h)** The frequency spectrums of release from transmitter and receiver. **(i)** The comparison of press and release frequency spectrums. **(j)** and **(k)** the voltage varies with distance of two coils from 0 cm to 100 cm. The inset is enlarged view of voltage from 5 cm to 100cm. **(l)**The frequency of different distance in press and release conditions.

than release after combining a switch. If a lower speed of pressing is applied, the output of press will decrease, and a more evident output boosting will be observed upon the closing of the switch.

Besides combining diode and switch together with the TENG to achieve an instantaneous discharging within the half cycle of the output, a single switch alone can accumulate charges in both pressing and releasing processes and generate two instantaneous peaks. Fig. 2(d) presents the one-switch method to enhance the positive and negative instantaneous output to 60 V and 120 V while the output of traditional-circuit-TENG is only at 34 V and 12 V, respectively. Meanwhile, the pulse widths for two half cycles are remarkably decreased to 18.2 ms and 9.7 ms, which means the signal frequency has been significantly enhanced. The working mechanism of instantaneous discharging to enhance output and frequency with a single switch is shown in Fig. S2. The enhanced signal frequency provides the feasibility for following direct wireless signal transmission without an external wireless module and external power source. In diversified practical applications, the most applicable method can be adopted from these three approaches according to different requirements.

Additionally, the dependence of absolute value of maximum voltage (V_{max}) on external load resistance is investigated and compared. Fig. 2 (e) shows that the voltage increases with external load resistances for traditional TENG while the voltage peak value does not vary with load resistance for other three circuit conditions according to equations (1) and (2). Thus, the power in Fig. 2(f) increases infinitely with decreased resistance while traditional TENG has an optimized power value and a large equivalent internal resistance around 10 MΩ, as shown in the inset of Fig. 2(f). In other words, instantaneous TENG has desirable output without impedance mismatch concern. All the three methods would be acceptable strategies to achieve frequency boost up by instantaneous discharging without impedance mismatch issue. They make the direct wireless transmission feasible even without external power supplier and additional wireless module.

3. The basic characterization of TENG-based direct wireless transmission

The one switch or switch-diode combination method offers high potential to realize direct wireless transmission. Theoretically, the instantaneous output would oscillate in a resonant circuit that consists of textile TENG, a single switch, and a coil with internal resistance. Hence, a high-frequency resonant signal can be generated in this way and then coupled to a receiver. To verify the capability of direct wireless TENG signal transmission, the basic characterization of textile TENG based wireless transmission is depicted in Fig. 3. The resonant frequency f of wireless TENG signal directly transmitted by RLC circuit is expressed by

$$f = \frac{1}{2\pi\sqrt{LC}} \tag{3}$$

Where L is the inductance value of the coil, C is the TENG capacitance. The resonant frequency is therefore mainly determined by the inductance of the coil, and the capacitance of the TENG. Thus, we first study the TENG capacitance in detail for subsequent frequency analysis of wireless resonant signal. Here we use the one-switch configuration to investigate the value of C_{press} and $C_{release}$ and their relationship, as shown in Fig. 3(a–c). The force 110 N measured by "*FlexiForce*" resistive force sensor (RFP803) is applied on textile TENG by hand press with the variation of 20 N. The detailed instantaneous discharging curves for press and release under load resistances 1 MΩ, 5 MΩ, 10 MΩ, and 20 MΩ are presented in Fig. 3(a). The voltage peak value keeps constant and pulse width (i.e. time constant) decreases when load resistance decreases. This trend is because the discharging process of one-switch TENG is similar with that of a capacitor. Therefore, the time constant τ is expressed by

$$\tau = RC \tag{4}$$

where R is the load resistance. Thus, the increased load resistance contributes a broadened bandwidth (i.e. larger time constant), but C_{press} and $C_{release}$ remain constant since the switch is closed only when textile TENG is pressed to lowermost and released to uppermost. Fig. 3(b) illustrates the detailed calculation of C_{press} and $C_{release}$, their value can be obtained from the exponentially decaying waveforms. This voltage profile can be described by the following equation [82].

$$V = V_{max} \cdot e^{-\frac{t}{\tau}} \tag{5}$$

where t is time, V_{max} is the absolute value maximum voltage. And the time constant τ which can be obtained from the waveform is normally defined as the time when V decreases from V_{max} to 1/e (36.8%) of V_{max}. Combining equations (4) and (5), the capacitance of press and release are calculated to be 1.82 nF and 0.97 nF when the load resistance is 10 MΩ, respectively. Similarly, the C_{press} and $C_{release}$ on different load resistances are calculated and summarized in Fig. 3(c). Based on equation (4), the time constant τ proportionally increases with the increased load resistance either under pressed or released, as indicated by blue lines in Fig. 3(c). The slopes of "Press" and "Release" remain constant as shown by red lines in Fig. 3(c), which indicates that C_{press} and $C_{release}$ do not vary with the load resistance but are determined by the contact surface area A and distance d between the two electrodes. This is also verified by the TENG capacitance vs load resistance. Because the d under pressed is smaller than that of the released state, C_{press} is larger than $C_{release}$ and the measured results show that the C_{press} is twice as much as $C_{release}$.

To directly transmit the resonant output of the textile TENG as it is pressed and released, a standard coil is connected to the textile TENG in series with the switch. Fig. 3(d) and (e) present the measurement set-up and equivalent wireless transmission circuit. The textile TENG is serially connected to a mechanical switch and a coil (inductance L = 1 mH) with internal resistance R_L to form the transmitter end. The receiver end is composed of a 1 nF capacitor to avoid the circuit mismatch between transmitter and receiver, a coil with the same specification as transmitter, and an oscilloscope connected to the end of receiver for measuring the oscillating signal inductively transferred from the transmitter. The distance between two coils varies from 0 cm (the two coils are placed as near as possible) to 100 cm which is the longest distance the receiver can still receive the signal. At the distance of 0 cm, the transmitted signals and the received signals as the textile TENG is pressed and released are depicted in Fig. 3(f). The corresponding normalized Fast Fourier transform (FFT) spectrums under pressed and released states are shown in Fig. 3(g) and (h). The signals of press from transmitter and receiver have similar resonant frequencies around 115 KHz. Similarly, the signals of release from transmitter and receiver also have similar resonant frequencies around 172 KHz. Based on equation (3), the theoretically calculated resonant frequency for press f_{press} and release $f_{release}$ is around 118 KHz and 161 KHz (C_{press}: 1.82 nF, $C_{release}$: 0.97 nF, L:1 mH), which is in good accordance with experimental results. Besides of that, the ratio of $C_{press}/C_{release}$ is 2 as mentioned in Fig. 3(c), leading to the ratio of $f_{press}/f_{release}$ is around $\sqrt{2}$ based on equation (3), as shown in Fig. 3(j). Thus, the source of the received oscillating signal is theoretically and experimentally confirmed from the textile TENG as it is pressed or released. As the transmitting distance increases from 0 cm to 100 cm, the received signal amplitude from both pressed state and released state decreases due to the increased energy loss in air (Fig. 3(j) and (k)). However, the resonant frequency of the received signals shows a good consistency as the distance increases for both pressed and released conditions as shown in Fig. 3(l), which has verified the stability of the direct TENG-based transmitted resonant signal over varying distances. These results have indicated the potential of the direct wireless transmission for wireless force sensing using the stable frequency as the sensing parameter.

4. The static force sensing based on resonant frequency shift

Up to now, various self-powered wireless TENG sensor networks have been reported [84–86]. Nevertheless, most of them separate the sensing and energy harvesting functions where the TENG only serves as a power source of additional wireless modules or works as sensor nodes. Meanwhile, the amplitude of TENG signal used for sensing purpose is susceptible to humidity, which restricts the expansion of applications of wireless self-powered TENG system. These two aspects are considered as large limitations of the TENG wireless sensor towards a stable and zero-power sensing system. To overcome the drawbacks of TENG signal instability coming from the amplitude variation, wireless TENG sensor based on resonant RLC circuit has been explored. A wireless TENG was reported [60] by using RLC circuit and laser diode for long-distance transmission, however, using laser diode did not achieve the real direct resonant signal wireless transmission. Moreover, the switch was integrated with TENG structure, which hinders free capacitance change and cannot harness steady resonant frequency shift to demonstrate stable sensing capabilities. In other words, it still depends on the amplitude change to achieve sensing purpose. Herein, we propose the direct TENG-based wireless transmission of the resonant signal that not only is battery-free but also contains the sensory information by using the resonant frequency shift as the sensory information that is largely resistant to the environmental interference such as humidity.

The one-switch approach is used to investigate the feasibility of wireless force sensing. Fig. 4 shows the force sensing based on resonant frequency shift mechanism and the distance of transmitter and receiver is 5 cm. Here the standard weights are gently put on the textile TENG and their gravities are used as the applied force to ensure the mechanical stimuli steady. Fig. 4(a) depicts the time-domain oscillating signal sunder different forces. The frequency-domain FFT signals are summarized in Fig. 4(b). As the force increases, the resonant frequency continuously shifts to lower values, as shown in the inset of Fig. 4(b). This is because increased force induces larger capacitance of the TENG. According to equation (3), increased capacitance causes smaller resonant frequency. The resonant frequency of each force is summarized in Fig. 4(c). A good linear range (0.5N–10 N) is observed with good sensitivity 434.7 Hz N^{-1}. When force increases to 10 N, two triboelectric layers tightly contact. The TENG capacitance cannot show a considerable change anymore, leading to the appearance of saturation range. The sensing stability under different relative humidity is investigated shown in Fig. 4(c). When relative humidity is 49.27%, 58.63%, 71.49%, three lines majorly overlap, and the resonant frequency of same force maintains similar. The results reveal that good anti-interference capability of resonant frequency signal is reliable and preferable for force or pressure sensing functions. It creates the possibility to prevent from the side effect of environment and remarkably improves the stability of TENG sensing system. Comparably, the normalized amplitude of resonant frequency-domain signal is influenced by relative humidity as shown in Fig. 4(d). Higher humidity lowers the amplitude of resonant frequency spectrum. In addition, there are two linear ranges. One is within 0.5N–10 N, another is within 10N–40 N. The slope of tiny-force range is higher than that of large-force area. The two different-slope linear ranges agree with the resonant frequency variation trend in Fig. 4(c), which indicates the amplitude of press with different force is mainly determined by the TENG capacitance while the applied force has little effect on the trend of relatively sharp increase by following a slowdown-increase. Meaningfully, Fig. 4(c) associated with Fig. 4(d) provides comprehensive information to obtain the external force and humidity simultaneously according to measured resonant frequency and normalized amplitude value. Similarly, the case for release is also discussed in Fig. 4(e–h). The voltage of time-domain oscillating signal increases as force increases, which follows the same trend as press case. However, the resonant frequency remains steady even at changing forces, which is shown in Fig. 4(f) and its inset and Fig. 4(g). This phenomenon can be easily expressed by the switch closing episode. No matter how the force changes, closing switch always happens at releasing to uppermost. Each operation cycle has the same final state, resulting same TENG capacitance which contributes to the changeless resonant frequency. In release case, the normalized amplitude of resonant frequency-domain signal is also influenced by relative humidity as shown in Fig. 4(h). It follows the trend that normalized amplitude increases with force and declines with relative humidity. Dissimilar with press case in Fig. 4(d), only the influence of force is responsible for two different-slope linear ranges without contribution of change rate of TENG capacitance. Thus, the normalized amplitude changes more obviously in large force area than tiny force area.

To demonstrate the static force sensing capabilities of this wireless network in real life, this system is used to perform the function of a wireless real-time electronic scale. The schematic diagram of sensing system is presented in Fig. 5(a). As mentioned before, the release case is not sensitive to force change. And it is not necessary for force sensing realization. Thus, forward diode approach is used to filter the release signal. A tray is put on the device for a uniform weight distribution on the object and then TENG device is connected to the transmitter coil. When objects with different weights are put on the scale, the press signal

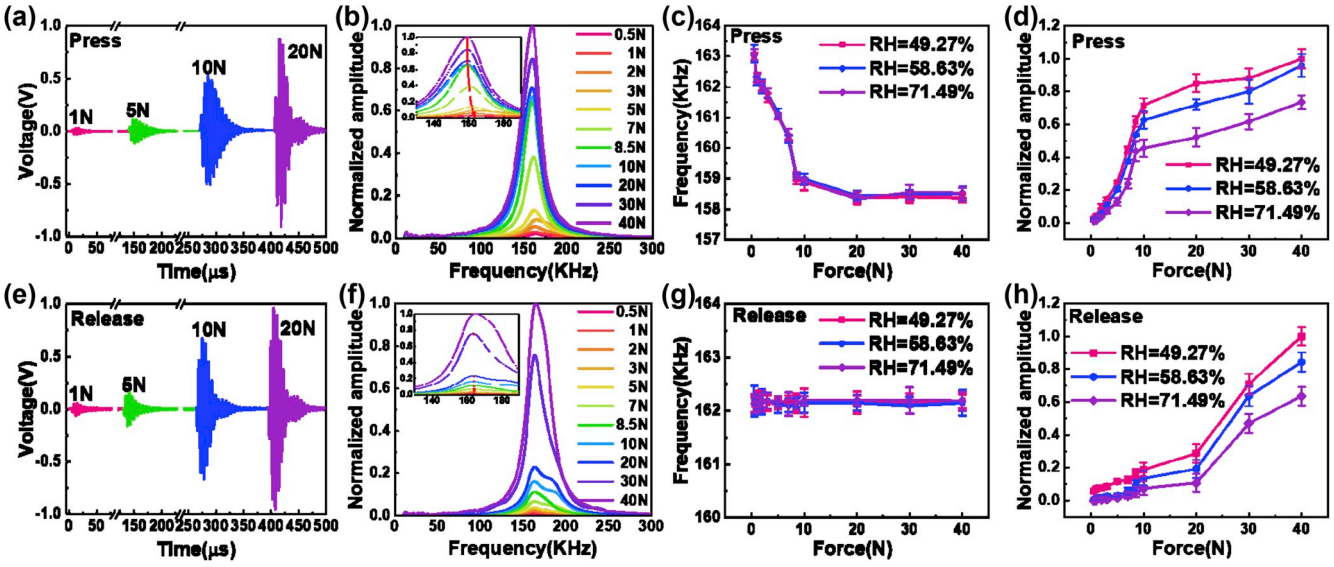

Fig. 4. Dependence of received signal frequency spectrum on force and humidity in the condition of press **(a) (b) (c) (d)** and release **(e) (f) (g) (h)**.

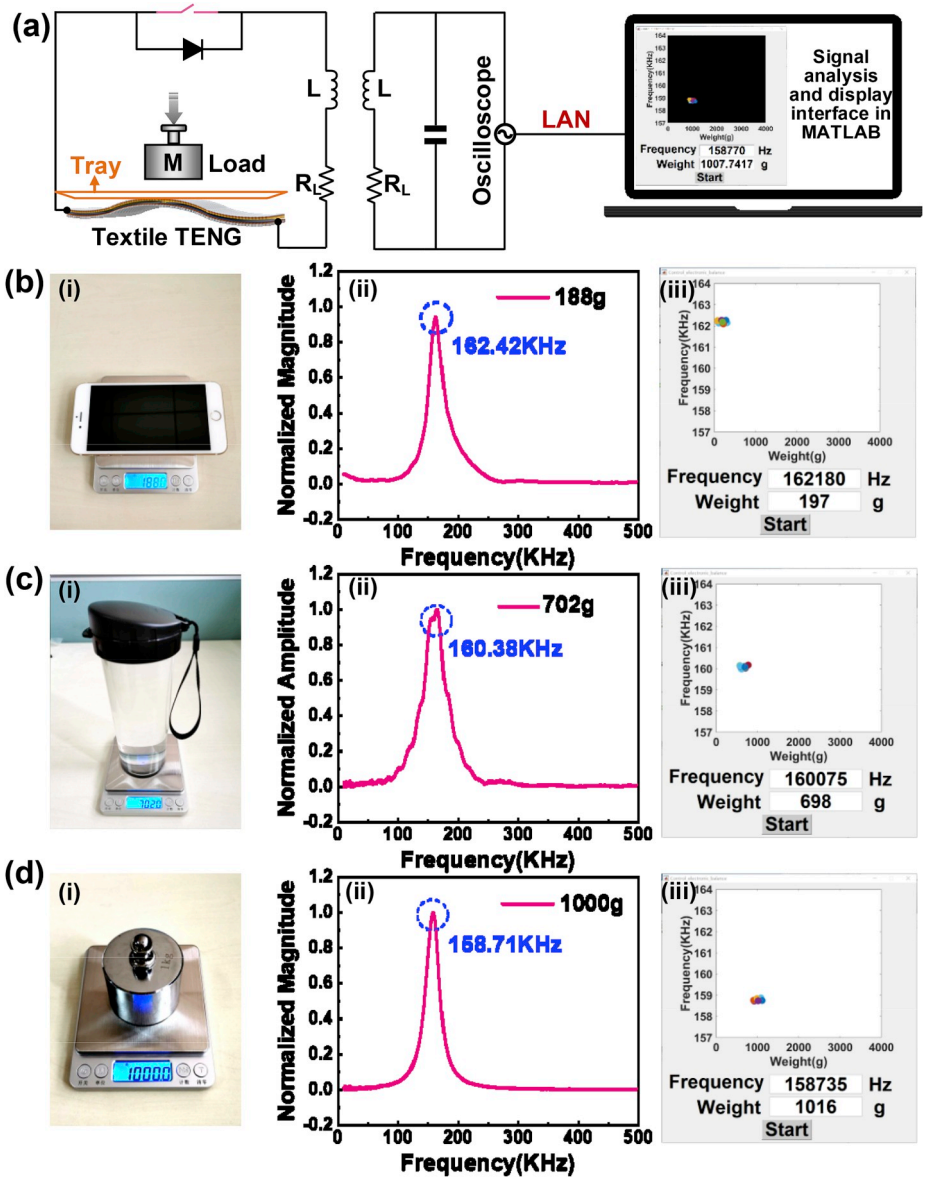

Fig. 5. The electronic scale application. **(a)** The system diagram of the wireless electronic scale. The calibrated weight (i), frequency spectrum (ii) and real-time weight displaying (iii) of mobile phone **(b)**, bottle with water **(c)** and 1 kg weight **(d)**.

is coupled on the receiver coil in the moment of closing switch. Due to the high resonant frequency characteristic of oscillating signal, the signal is acquired by an oscilloscope that serves as the high-speed data acquisition equipment. Accordingly, in Fig. 5(a), we build a communication interface between oscilloscope and signal analysis software MATLAB based on local area network (LAN), next MATLAB extracts the resonant signal from oscilloscope to perform real-time FFT analysis and obtain the resonant frequency. According to the linear relationship between force and resonant frequency in Fig. 4(c), MATLAB calculates the corresponding weight of each object and displays on the computer screen. Fig. 5(b–d) shows different object weights, corresponding frequency-domain signals and display interface, including a mobile phone (188 g), bottle filled with water (702 g), and weight (1000 g), by using commercialized scale for comparison and verification. As the weight interface displays, the measured weights, 197 g for mobile phone, 698 g for water bottle and 1016 g for weight, indicate a relatively good consistency with commercialized scale. Video S1 shows the weighing 5 times for each object. Then the results of 5 times weighing are summarized in Supplementary Information Table S1, slight error percentage between commercialized scale and our work indicates good force sensing feasibility of our wireless scale system. Moreover, heavier object shows lower resonant frequency, which is in accordance with force calibration curve in Fig. 4(c). In this scenario, the fore-end, transmitter, acts not only sensors carried sensory information as mentioned before, but also power source provided by TENG itself, which realizes a fully battery-free self-powered wireless TENG system. The short-range wireless sensory transmission system is beneficial from the power free of front ends, reducing the overall power consumptions of the wireless system, which is preferable for IoT networks.

Supplementary video related to this article can be found at https://doi.org/10.1016/j.nanoen.2019.104266.

5. Wireless toy car control

HMIs penetrate our daily life in many aspects such as VR game and smart home, great market demand promotes the rapid progress of the HMI since the last decades. Reported flexible HMIs [23,87] based on TENG signal amplitude enhance the user experience in human machine

interactions. However, the resonant frequency-shift based control applications are rarely reported. The resonant frequency signal is quite stable, which is highly desirable for diversified control applications. By adopting the parallel or series connection of textile TENG, distinguished resonant frequency between press and release can generate three freedom degrees, which is adequate and reasonable for 2D toy car control. Fig. 6(a) shows the schematic diagram of the wireless car control system. The three freedom degrees, including parallel connection of press (forward), parallel connection of release (backward), series connection of press (left rotation) and series connection of release (right rotation), are distributed to four pixels respectively. The four pixels are connected to the same coil whose inductance value is 1 mH and distance of two coils remains 5 cm, then the mechanical force induced current of TENG generates an oscillating signal in RLC circuit. Detailed circuit in dashed line is forward diode for press case and reversed diode for release case. Through direct inductive coupling, the oscillating signal which is acquired by oscilloscope is coupled onto receiver ends. Consecutive real-time reading and FFT analysis are performed by MATLAB. Based on Bluetooth communication interface, MATLAB sends an order which corresponds to the specific resonant frequency, to the car for executing different speeds of forward/backward/left rotation/right rotation movements. Small force and large force induced intensity of normalized amplitude is defined to link with the speed of car. It is noted that small and large force are all within saturation range of force calibration curve in Fig. 4(c) as to reduce variables through keeping resonant frequency constant. As shown in Fig. 6(b) and (c), 125.4 KHz is obtained from the signal of parallel connection of press and corresponding order makes car high and slow speed forward according to the normalized amplitude. In a similar way, the resonant frequency of parallel connection of release 164.2 KHz is used to make car move backward as shown in Fig. 6(d) and (e). If the parallel connection of textile TENG is converted to series way, the C_{press} and $C_{release}$ are decreased to one-quarter of parallel case, so the resonant frequency is remarkably increased to 338.2 KHz and 465.1 KHz respectively according to equation (3). Thus, evident characteristics can be differentiated among these four pixels. Fig. 6(f–i) presents that 338.2 KHz and 465.1 KHz control the movements of left and right rotation, respectively. The rotation speed adjustment can be realized by the amplitude of FFT signal. Small amplitude is defined as low rotation speed and large amplitude is corresponding to high rotation speed. A video showing car control is provided by Video S2. This control scenario demonstrates the feasibility of direct real-time wireless control by TENG based SS-WSN based on resonant frequency shift mechanism.

Supplementary video related to this article can be found at https://doi.org/10.1016/j.nanoen.2019.104266.

6. Wireless 3D VR drone control

Nowadays, Augment reality (AR) and virtual reality (VR) become more and more popular in the human-machine interaction. The general virtual game usually relies on visual communication. As an alternative method, direct TENG based wireless signal transmission, provides a new interaction approach and extend the choices of communication methods for HMIs. As mentioned earlier, except the freedom degree generated by alternating the connection of textile TENG itself, the external circuit adjustment is a strategic approach to increase the number of freedom degree to realize more systematic and comprehensive 3D VR control such as drone control. In this way, we do not change the connection method of textile TENG but parallel connect a specific capacitor $C_{control}$ which varies from 0 nF to 15 nF to achieve resonant frequency differentiations of freedom degrees under parallel connection of textile TENG as shown in Fig. 7(b). A single signal is enough to serve as the trigger signal to initiate drone movement. Thus, a forward diode with single switch combination is again used to bypass the release signal and simplifying the system design as only the press signal matters. The system control diagram is presented in Fig. 7(a). A smart mat with 8 pixels, where each of them is 8*8 cm^2 and in a configuration of 4 pieces to enhance the transmission efficiency, is connected to a single transmitter coil. The receiver obtains 8 differentiated signals which are acquired by oscilloscope, and then is extracted by MATLAB based on LAN communication. Through FFT analysis, distinguished resonant frequency of each pixel is obtained and defined as different drone movement commands, including forward, backward, left, right, up, down, left rotation, and right rotation. The drone in UNITY gets the order to fly to different directions. Fig. 7(c) and (d) show the resonant frequency

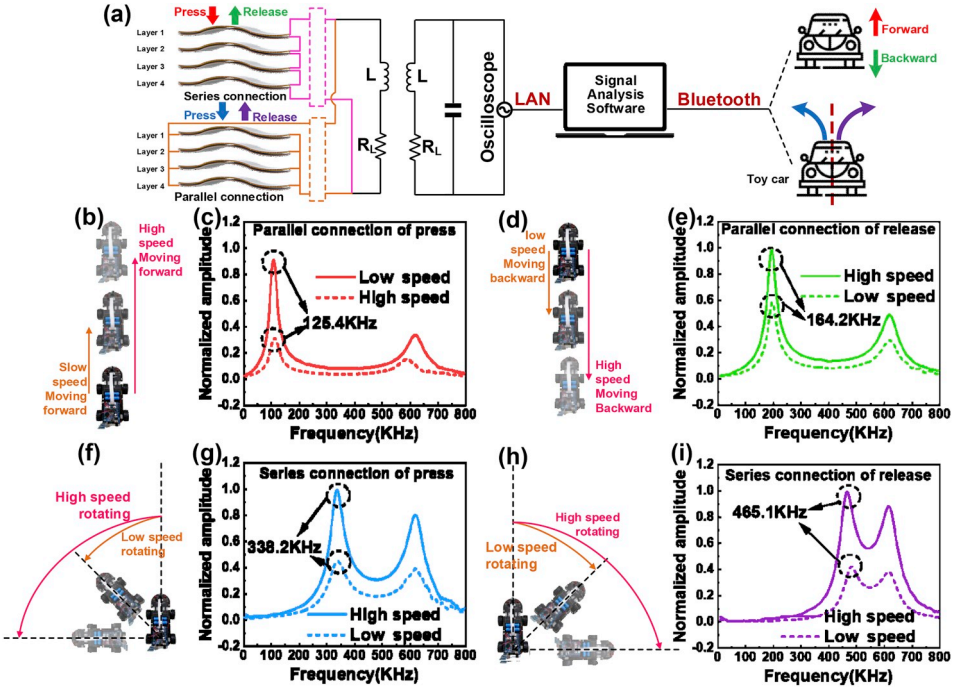

Fig. 6. Wireless toy car control. **(a)** The control system diagram of car. The frequency spectrum of forward **(b) (c)**, backward **(d) (e)**, the left rotation **(f) (g)** and right rotation **(h) (i)**.

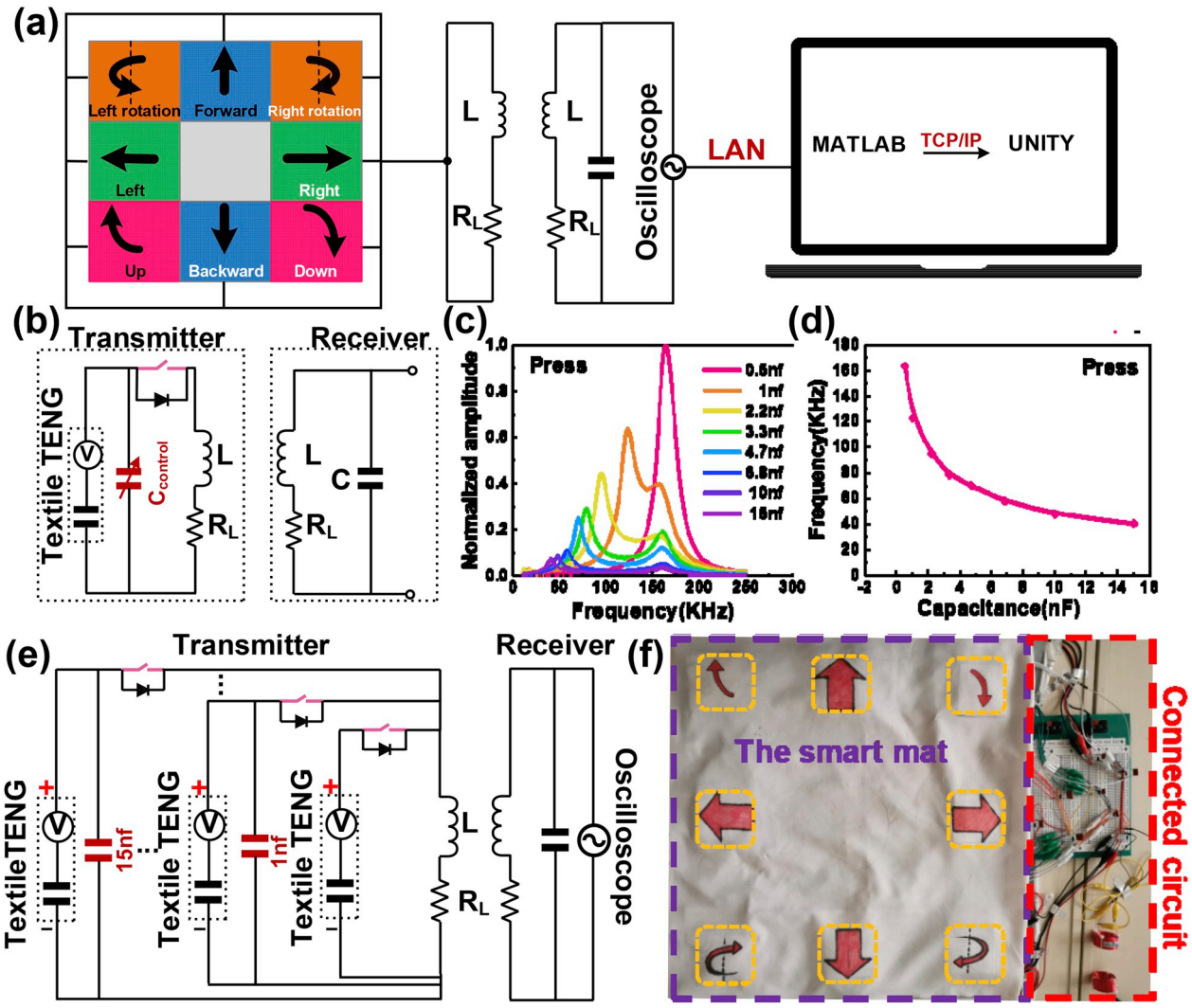

Fig. 7. **(a)** The real-time 3D VR drone control system diagram. **(b)** The equivalent circuit of single pixel. **(c)** The frequency spectrum with different capacitors. **(d)** The dependence of frequency on capacitors. **(e)** The equivalent circuit of the control smart mat. **(f)** The physical image of smart mat for drone control.

spectrum under different $C_{control}$, which corresponds to specific pixel and direction. The capacitance value from 0 nF to 15 nF is corresponding to resonant frequency from 163.7 KHz to 40.1 KHz. The equivalent circuit and image of smart mat are depicted in Fig. 7(e) and (f). Only one-pair transmitter and receiver are used in this smart control panel, which greatly simplifies the system architecture and avoid the synchronous alignment between multiple-pair transmitter and receiver to avoid misalignment induced energy lose. The smart mat with the area 60*60 cm^2 is in a 3*3 array where the most central location is designed as the people standing point. The detailed fabrication process can be found in experimental section.

The detailed drone control is summarized in Fig. 8. Fig. 8(a) and (c) are the overall layout of mat, such as directions and related capacitance values of $C_{control}$. The control circuit of individual pixel and coordinate system are diagramed in Fig. 8(b) and (d). The forward diode with switch is adopted as only the press signal is adequate to trigger the drone move. The resonant frequency of four-piece textile TENG under press case (0 nF) is 118 KHz-125KHz which overlaps with the resonant frequency of 1 nF capacitor, therefore this pixel is in two-piece configuration which refers to two textile TENGs stacked together as demonstrated in Fig. S3 to boost and conveniently differentiate resonant frequency. This pixel does not connect with external capacitor $C_{control}$ but relies on the device capacitance itself to produce resonant frequency information 163.7 KHz, controlling up action of drone. The oscillating signal from receiver and resonant frequency spectrum after FFT analysis are shown in Fig. 8(e)(i) and (ii), respectively. Fig. 8(e)(iii) and (iv) are relevant to down action of drone with 123.1 KHz. Similarly, Fig. 8(f–h) correspond to 6 drone directions, including left, right, forward, backward, right rotation and left rotation. Video S3 is provided to show the control process. The multiple-freedom-degree controls not only depend on the freedom degree created by textile TENG itself but also can be extended by external circuit adjustment. Thus, it is prospective to achieve more sophisticated and comprehensive control with large number of freedom degrees which may improve the human-machine interaction experience.

Supplementary video related to this article can be found at https://doi.org/10.1016/j.nanoen.2019.104266.

7. Conclusion

In summary, the SS-WSN that featured with battery-free, sensible and frequency-distinguishable characteristics is proposed by using TENG based direct sensory transmission (TDST) mechanism. By leveraging a switch, reduced pulse width that refers to boosted frequency of TENG signal is achieved by instantaneous discharging. It makes the direct TENG based wireless transmission feasible by simply connecting textile TENG to a coil without external power sources and wireless modules. The transmission range can be up to 1 m. Furthermore, the novel SS-WSN delivers wireless sensing function based on

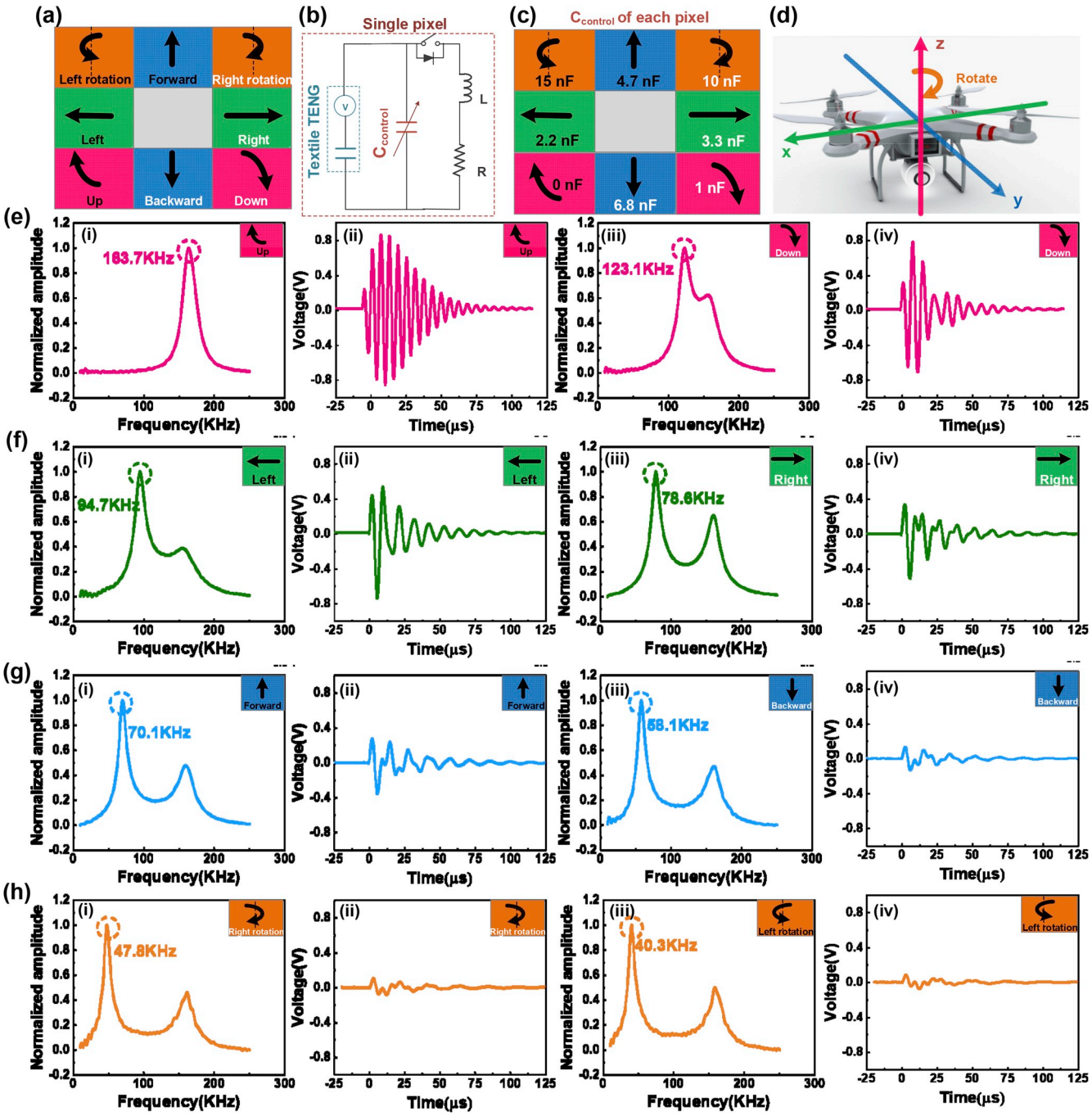

Fig. 8. Demonstration of eight-freedom-degree 3D drone VR control based on frequency difference. **(a)** Up. **(b)** Down. **(c)** Left. **(d)** Right. **(e)** Forward. **(f)** Backward. **(g)** Right rotation. **(h)** Left rotation.

distinguishable resonant frequencies without integration of external identity tags. Differentiated from previously reported works (Nano Energy, 51 (2018) 1–9), we use the distinguishable resonant frequency that is immune to the environmental variables such as humidity instead of signal amplitude to realize a highly sensitive force sensing with the benefits of soft textile TENG. As a practical application, a wireless electronic scale based on force sensing is realized, providing an effective way to measure the weight of different objects. Through varying the combinations of the TENG textile layer connection and the switch closing moment (i.e. as the textile TENG is pressed or released), a 2D toy car control is realized with three degrees of freedom. In addition, by adjusting the external capacitor to generate extra distinguishable resonant frequencies, a more sophisticated and comprehensive eight-freedom-degree 3D VR drone control is achieved. In future, the SS-WSN using TENG which serves as both power source and sensor simultaneously has brought new possibilities towards extended practical applications of IoT towards VR/AR human-machine interaction, healthcare, factory automation, and smart home in the future.

8. Experimental section

Fabrication of the textile-based narrow-gap TENG: the Ecoflex TM00-30 (the weight ratio of A/B is 1) is coated on the surface of commercially available conductive textile, which works as negative tribo-electrification layer. The positive layer is composed of wrinkle nitrile attached on the adhesive conductive textile electrode. Then non-

conductive textile is used as insulating layer to encapsulate electrodes. The one piece consists of a pair of triboelectrification layer (i.e. nitrile and Ecoflex), the electrodes and encapsulation layers. All the devices for measurements and applications are with the area 8*8 cm^2 and in 4-piece configuration except for special statement. To avoid relative sliding between layers, 4 pieces are stitched together.

Fabrication of the smart mat: A commercially available cushion with area 60*60 cm^2 is used as substrate for textile TENG array layout. Eight 4-piece TENG pixels stack with respective textile-based switch and are attached on the cushion into 3*3 array, the middle vacant area is for people standing point. Next, each pixel is connected to a forward diode, the same transmitter coil, and capacitor $C_{control}$. The signals of all pixels are also inductively coupled to the same receiver. Finally, an encapsulation layer with direction marks is attached on the cushion surface to make a functional and integrated smart mat as control interface.

Measurement and calibration of force: The force for the basic characterization of TENG-based direct wireless transmission was applied by hand press and calibrated by "*FlexiForce*" resistive force sensor (RFP803). The calibration data of the "*FlexiForce*" sensor is shown in Fig. S4.

Measurement of wireless signal: DPO5034B Oscilloscope from Tektronix is used to measure the oscillating signal from receiver. For force measurement, the sampling frequency is 20 MS/s, record length are 4,000 points, which can be conveniently processed and analyzed offline. For precision purpose, the record length 4,000 points are padded with 4,000,000 points according algorithm in MATLAB. The FFT frequency resolution ΔR is defined as:

$$\Delta R = \frac{f_s}{N}$$

Where f_s is the sampling frequency, N is the number of data points. According to the definition of ΔR, the FFT frequency resolution is 5,000 Hz before the data point is zero padded to 4,000,000 by algorithm in MATLAB. However, the sensitivity of force sensing is 434.7 $Hz.N^{-1}$. The resonant frequency shift is hardly observed or recognized by ORIGIN even the textile TENG experiences large force variation (e.g. 10 N) because induced frequency shift is 4347Hz which is smaller than the FFT frequency resolution 5,000Hz. Zero padding in the tail of time-domain signal provides a convenient way to enhance the FFT frequency resolution without changing the characteristics of wireless signal. Thus, the 4,000 data points acquired from oscilloscope are conveniently padded to 4,000,000 in MATLAB where the FFT resolution frequency is enhanced to 5 Hz which is precise enough for slight resonant frequency shift recognition of the force sensing. Besides, the sampling frequency for control is 5 MS/s and record length are 5,000 points, resulting frequency resolution is 1000Hz. This sampling frequency is proper for real-time FFT analysis in MATLAB to reduce control delay since the differentiation between control signals is obvious.

Declaration of competing interest

The authors declare that they have no known competing financial interests or personal relationships that could have appeared to influence the work reported in this paper.

Acknowledgements

F.W., H.W. and T.H. contributed equally to this work. This work was supported by HiFES Seed Funding-2017-01 grant (R-263-501-012-133) "Hybrid Integration of Flexible Power Source and Pressure Sensors" at the National University of Singapore; NRF-ISF Joint Research Grant (NRF-ISF) (NRF2015-NRF-ISF001-2620); Agency for Science, Technology and Research (A*STAR), Singapore and Narodowe Centrum Badań i Rozwoju (NCBR), Poland Joint Grant (R-263-000-C91-305) "Chip-Scale MEMS Micro Spectrometer for Monitoring Harsh Industrial Gases".

Appendix A. Supplementary data

Supplementary data to this article can be found online at https://doi.org/10.1016/j.nanoen.2019.104266.

References

[1] S. Niu, N. Matsuhisa, L. Beker, J. Li, S. Wang, J. Wang, Y. Jiang, X. Yan, Y. Yun, W. Burnett, A wireless body area sensor network based on stretchable passive tags, Nat. Electron. 2 (2019) 361–368.
[2] B. Chu, W. Burnett, J.W. Chung, Z. Bao, Bring on the bodyNET, Nat. News 549 (2017) 328.
[3] Y. Chen, Y.C. Wang, Y. Zhang, H. Zou, Z. Lin, G. Zhang, C. Zou, Z.L. Wang, Elastic-beam triboelectric nanogenerator for high-performance multifunctional applications: sensitive scale, acceleration/force/vibration sensor, and intelligent keyboard, Adv. Energy Mater. 8 (2018) 1802159.
[4] C. Wu, A.C. Wang, W. Ding, H. Guo, Z.L. Wang, Triboelectric nanogenerator: a foundation of the energy for the new era, Adv. Energy Mater. 9 (2019) 1802906.
[5] S. Lee, Q. Shi, C. Lee, From flexible electronics technology in the era of IoT and artificial intelligence toward future implanted body sensor networks, Apl. Mater. 7 (2019), 031302.
[6] M.F. Farooqui, M.A. Karimi, K.N. Salama, A. Shamim, 3D-Printed disposable wireless sensors with integrated Microelectronics for large area environmental monitoring, Adv. Mater. Technol. 2 (2017) 1700051.
[7] K. Zhao, Z.L. Wang, Y. Yang, Self-powered wireless smart sensor node enabled by an ultrastable, highly efficient, and superhydrophobic-surface-based triboelectric nanogenerator, ACS Nano 10 (2016) 9044–9052.
[8] S.S. Gill, P. Garraghan, R. Buyya, ROUTER: fog enabled cloud based intelligent resource management approach for smart home IoT devices, J. Syst. Softw. 154 (2019) 125–138.
[9] J. Wen, B. Chen, W. Tang, T. Jiang, L. Zhu, L. Xu, J. Chen, J. Shao, K. Han, W. Ma, Harsh-environmental-resistant triboelectric nanogenerator and its applications in autodrive safety warning, Adv. Energy Mater. 8 (2018) 1801898.
[10] S. Han, J. Kim, S.M. Won, Y. Ma, D. Kang, Z. Xie, K.-T. Lee, H.U. Chung, A. Banks, S. Min, Battery-free, wireless sensors for full-body pressure and temperature mapping, Sci. Transl. Med. 10 (2018), eaan4950.
[11] L. Wang, W.A. Daoud, Highly flexible and transparent polyionic-skin triboelectric nanogenerator for biomechanical motion harvesting, Adv. Energy Mater. 9 (2019) 1803183.
[12] K.H. Koh, Q. Shi, S. Cao, D. Ma, H.Y. Tan, Z. Guo, C. Lee, A self-powered 3D activity inertial sensor using hybrid sensing mechanisms, Nano Energy 56 (2019) 651–661.
[13] J. Wang, H. Wang, C. Lee, Mechanism and applications of electrical stimulation disturbance on motoneuron excitability studied using flexible intramuscular electrode, Adv. Biosyst. 3 (2019) 1800281.
[14] S. Lee, H. Wang, W.Y.X. Peh, T. He, S.-C. Yen, N.V. Thakor, C. Lee, Mechano-neuromodulation of autonomic pelvic nerve for underactive bladder: a triboelectric neurostimulator integrated with flexible neural clip interface, Nano Energy 60 (2019) 449–456.
[15] A.P. Gerratt, H.O. Michaud, S.P. Lacour, Elastomeric electronic skin for prosthetic tactile sensation, Adv. Funct. Mater. 25 (2015) 2287–2295.
[16] S. Takamatsu, T. Lonjaret, E. Ismailova, A. Masuda, T. Itoh, G.G. Malliaras, Wearable keyboard using conducting polymer electrodes on textiles, Adv. Mater. 28 (2016) 4485–4488.
[17] Q. Shi, Z. Zhang, T. Chen, C. Lee, Minimalist and multi-functional human machine interface (HMI) using a flexible wearable triboelectric patch, Nano Energy 62 (2019) 355–366.
[18] T. Chen, Q. Shi, M. Zhu, T. He, Z. Yang, H. Liu, L. Sun, L. Yang, C. Lee, Intuitive-augmented human-machine multidimensional nano-manipulation terminal using triboelectric stretchable strip sensors based on minimalist design, Nano Energy 60 (2019) 440–448.
[19] T. Chen, Q. Shi, M. Zhu, T. He, L. Sun, L. Yang, C. Lee, Triboelectric self-powered wearable flexible patch as 3D motion control interface for robotic manipulator, ACS Nano 12 (2018) 11561–11571.
[20] K. Dong, X. Peng, Z.L. Wang, Fiber/fabric-based piezoelectric and triboelectric nanogenerators for flexible/stretchable and wearable electronics and artificial intelligence, Adv. Mater. (2019) 1902549.
[21] Q. Shi, C. Qiu, T. He, F. Wu, M. Zhu, J.A. Dziuban, R. Walczak, M.R. Yuce, C. Lee, Triboelectric single-electrode-output control interface using patterned grid electrode, Nano Energy 60 (2019) 545–556.
[22] Q. Shi, T. He, C. Lee, More than energy harvesting-Combining triboelectric nanogenerator and flexible electronics technology for enabling novel micro-/nano-systems, Nano Energy 57 (2019) 851–871.
[23] T. He, Z. Sun, Q. Shi, M. Zhu, D.V. Anaya, M. Xu, T. Chen, M.R. Yuce, A.V.-Y. Thean, C. Lee, Self-powered glove-based intuitive interface for diversified control applications in real/cyber space, Nano Energy 58 (2019) 641–651.
[24] Q. Shi, C. Lee, Self-powered bio-inspired spider-net-coding interface using single electrode triboelectric nanogenerator, Adv. Sci. (2019) 1900617.
[25] A. Yu, X. Chen, R. Wang, J. Liu, J. Luo, L. Chen, Y. Zhang, W. Wu, C. Liu, H. Yuan, Triboelectric nanogenerator as a self-powered communication unit for processing and transmitting information, ACS Nano 10 (2016) 3944–3950.
[26] W. Ding, C. Wu, Y. Zi, H. Zou, J. Wang, J. Cheng, A.C. Wang, Z.L. Wang, Self-powered wireless optical transmission of mechanical agitation signals, Nano Energy 47 (2018) 566–572.

[27] A. Ahmed, Z. Saadatnia, I. Hassan, Y. Zi, Y. Xi, X. He, J. Zu, Z.L. Wang, Self-powered wireless sensor node enabled by a duck-shaped triboelectric nanogenerator for harvesting water wave energy, Adv. Energy Mater. 7 (2017) 1601705.

[28] X. Zhao, G. Wei, X. Li, Y. Qin, D. Xu, W. Tang, H. Yin, X. Wei, L. Jia, Self-powered triboelectric nano vibration accelerometer based wireless sensor system for railway state health monitoring, Nano Energy Nano Environ. 34 (2017) 549–555.

[29] Y. Wu, Y. Hu, Z. Huang, C. Lee, F. Wang, Electret-material enhanced triboelectric energy harvesting from air flow for self-powered wireless temperature sensor network, Sens. Actuators A Phys. 271 (2018) 364–372.

[30] S.S. Kwak, H.J. Yoon, S.W. Kim, Mechanical energy harvesting: textile-based triboelectric nanogenerators for self-powered wearable electronics, Adv. Funct. Mater. 29 (2019) 1970011.

[31] S.S. Kwak, H.J. Yoon, S.W. Kim, Textile-based triboelectric nanogenerators for self-powered wearable electronics, Adv. Funct. Mater. 29 (2019) 1804533.

[32] M. Zhu, Q. Shi, T. He, Z. Yi, Y. Ma, B. Yang, T. Chen, C. Lee, Self-powered and self-functional cotton sock using piezoelectric and triboelectric hybrid mechanism for healthcare and sports monitoring, ACS Nano 13 (2019) 1940–1952.

[33] W. Jiang, H. Li, Z. Liu, Z. Li, J. Tian, B. Shi, Y. Zou, H. Ouyang, C. Zhao, L. Zhao, Fully bioabsorbable natural materials based triboelectric nanogenerators, Adv. Mater. 30 (2018) 1801895.

[34] T. He, Q. Shi, H. Wang, F. Wen, T. Chen, J. Ouyang, C. Lee, Beyond energy harvesting-multi-functional triboelectric nanosensors on a textile, Nano Energy 57 (2019) 338–352.

[35] M. Gao, C.K. Peh, H.T. Phan, L. Zhu, G.W. Ho, Solar absorber gel: localized macro-nano heat channeling for efficient plasmonic Au nanoflowers photothermic vaporization and triboelectric generation, Adv. Energy Mater. 8 (2018) 1800711.

[36] J. Xiong, P. Cui, X. Chen, J. Wang, K. Parida, M.-F. Lin, P.S. Lee, Skin-touch-actuated textile-based triboelectric nanogenerator with black phosphorus for durable biomechanical energy harvesting, Nat. Commun. 9 (2018) 4280.

[37] K. Nan, S.D. Kang, K. Li, K.J. Yu, F. Zhu, J. Wang, A.C. Dunn, C. Zhou, Z. Xie, M. T. Agne, Compliant and stretchable thermoelectric coils for energy harvesting in miniature flexible devices, Sci. Adv. 4 (2018), eaau5849.

[38] T. Soyata, L. Copeland, W. Heinzelman, RF energy harvesting for embedded systems: a survey of tradeoffs and methodology, IEEE Circuits Syst. Mag. 16 (2016) 22–57.

[39] J. Gubbi, R. Buyya, S. Marusic, M. Palaniswami, Internet of Things (IoT): a vision, architectural elements, and future directions, Future Gener. Comput. Syst. 29 (2013) 1645–1660.

[40] E.J. Lee, T.Y. Kim, S.-W. Kim, S. Jeong, Y. Choi, S.Y. Lee, High-performance piezoelectric nanogenerators based on chemically-reinforced composites, Energy Environ. Sci. 11 (2018) 1425–1430.

[41] S. Qin, Q. Zhang, X. Yang, M. Liu, Q. Sun, Z.L. Wang, Hybrid piezo/triboelectric-driven self-charging electrochromic supercapacitor power package, Adv. Energy Mater. 8 (2018) 1800069.

[42] T. Li, J. Zou, F. Xing, M. Zhang, X. Cao, N. Wang, Z.L. Wang, From dual-mode triboelectric nanogenerator to smart tactile sensor: a multiplexing design, ACS Nano 11 (2017) 3950–3956.

[43] Q. Zheng, B. Shi, Z. Li, Z.L. Wang, Recent progress on piezoelectric and triboelectric energy harvesters in biomedical systems, Adv. Sci. 4 (2017) 1700029.

[44] X. Wang, Y. Yang, Effective energy storage from a hybridized electromagnetic-triboelectric nanogenerator, Nano Energy 32 (2017) 36–41.

[45] H. Liu, C. Hou, J. Lin, Y. Li, Q. Shi, T. Chen, L. Sun, C. Lee, A non-resonant rotational electromagnetic energy harvester for low-frequency and irregular human motion, Appl. Phys. Lett. 113 (2018) 203901.

[46] J. Chung, H. Yong, H. Moon, S.T. Choi, D. Bhatia, D. Choi, D. Kim, S. Lee, Capacitor integrated triboelectric nanogenerator based on metal metal contact for current amplification, Adv. Energy Mater. 8 (2018) 1703024.

[47] Y. Xi, H. Guo, Y. Zi, X. Li, J. Wang, J. Deng, S. Li, C. Hu, X. Cao, Z.L. Wang, Multifunctional TENG for blue energy scavenging and self-powered wind-speed sensor, Adv. Energy Mater. 7 (2017) 1602397.

[48] R. Hinchet, H.-J. Yoon, H. Ryu, M.-K. Kim, E.-K. Choi, D.-S. Kim, S.-W. Kim, Transcutaneous ultrasound energy harvesting using capacitive triboelectric technology, Science 365 (2019) 491–494.

[49] Y. Liu, N. Sun, J. Liu, Z. Wen, X. Sun, S.-T. Lee, B. Sun, Integrating a silicon solar cell with a triboelectric nanogenerator via a mutual electrode for harvesting energy from sunlight and raindrops, ACS Nano 12 (2018) 2893–2899.

[50] Y. Yang, N. Sun, Z. Wen, P. Cheng, H. Zheng, H. Shao, Y. Xia, C. Chen, H. Lan, X. Xie, Liquid-metal-based super-stretchable and structure-designable triboelectric nanogenerator for wearable electronics, ACS Nano 12 (2018) 2027–2034.

[51] Q. Shen, X. Xie, M. Peng, N. Sun, H. Shao, H. Zheng, Z. Wen, X. Sun, Self-powered vehicle emission testing system based on coupling of triboelectric and chemoresistive effects, Adv. Funct. Mater. 28 (2018) 1703420.

[52] H. Yang, Y. Pang, T. Bu, W. Liu, J. Luo, D. Jiang, C. Zhang, Z.L. Wang, Triboelectric micromotors actuated by ultralow frequency mechanical stimuli, Nat. Commun. 10 (2019) 2309.

[53] C. Zhang, T. Bu, J. Zhao, G. Liu, H. Yang, Z.L. Wang, Tribotronics for active mechanosensation and self-powered microsystems, Adv. Funct. Mater. (2019) 1808114.

[54] Q. Shi, H. Wu, H. Wang, H. Wu, C. Lee, Self-powered gyroscope ball using a triboelectric mechanism, Adv. Energy Mater. 7 (2017) 1701300.

[55] F. Fan, Z. Tian, Z. Wang, Flexible triboelectric generator, Nano Energy 1 (2012) 328–334.

[56] B. Nie, R. Huang, T. Yao, Y. Zhang, Y. Miao, C. Liu, J. Liu, X. Chen, Textile based wireless pressure sensor array for human interactive sensing, Adv. Funct. Mater. (2019) 1808786.

[57] J. Zou, M. Zhang, J. Huang, J. Bian, Y. Jie, M. Willander, X. Cao, N. Wang, Z. L. Wang, Coupled supercapacitor and triboelectric nanogenerator boost biomimetic pressure sensor, Adv. Energy Mater. 8 (2018) 1702671.

[58] S.W. Chen, X. Cao, N. Wang, L. Ma, H.R. Zhu, M. Willander, Y. Jie, Z.L. Wang, An ultrathin flexible single-electrode triboelectric-nanogenerator for mechanical energy harvesting and instantaneous force sensing, Adv. Energy Mater. 7 (2017) 1601255.

[59] K. Xu, S. Li, S. Dong, S. Zhang, G. Pan, G. Wang, L. Shi, W. Guo, C. Yu, J. Luo, Bioresorbable electrode array for electrophysiological and pressure signal recording in the brain, Adv. Healthc. Mater. (2019) 1801649.

[60] S. Park, S. Ahn, J. Sun, D. Bhatia, D. Choi, K.S. Yang, J. Bae, J.J. Park, Highly bendable and rotational textile structure with prestrained conductive sewing pattern for human Joint monitoring, Adv. Funct. Mater. 29 (2019) 1808369.

[61] S.L. Zhang, Y.C. Lai, X. He, R. Liu, Y. Zi, Z.L. Wang, Auxetic foam based contact mode triboelectric nanogenerator with highly sensitive self-powered strain sensing capabilities to monitor human body movement, Adv. Funct. Mater. 27 (2017) 1606695.

[62] M. Xu, P. Wang, Y.C. Wang, S.L. Zhang, A.C. Wang, C. Zhang, Z. Wang, X. Pan, Z. L. Wang, A soft and robust spring based triboelectric nanogenerator for harvesting arbitrary directional vibration energy and self-powered vibration sensing, Adv. Energy Mater. 8 (2018) 1702432.

[63] C. Hou, T. Chen, Y. Li, M. Huang, Q. Shi, H. Liu, L. Sun, C. Lee, A rotational pendulum based electromagnetic/triboelectric hybrid generator for ultra-low-frequency vibrations aiming at human motion and blue energy applications, Nano Energy 63 (2019) 103871.

[64] Z. Wang, S. Yang, S. Miao, Q. Shi, T. He, C. Lee, A motion-balanced sensor based on the triboelectricity of nano-iron suspension and flexible polymer, Nanomaterials 9 (2019) 690.

[65] H. Guo, X. Pu, J. Chen, Y. Meng, M.-H. Yeh, G. Liu, Q. Tang, B. Chen, D. Liu, S. Qi, A highly sensitive, self-powered triboelectric auditory sensor for social robotics and hearing aids, Sci. Robot. 3 (2018) eaat2516.

[66] P. Jiang, L. Zhang, H. Guo, C. Chen, C. Wu, S. Zhang, Z.L. Wang, Signal output of triboelectric nanogenerator at oil–water–solid multiphase interfaces and its application for dual signal chemical sensing, Adv. Mater. (2019) 1902793.

[67] J. Wang, H. Wang, N.V. Thakor, C. Lee, Self-powered direct muscle stimulation using a triboelectric nanogenerator (TENG) integrated with a flexible multiple-channel intramuscular electrode, ACS Nano 13 (2019) 3589–3599.

[68] C. Sun, Q. Shi, D. Hasan, M.S. Yazici, M. Zhu, Y. Ma, B. Dong, Y. Liu, C. Lee, Self-powered multifunctional monitoring system using hybrid integrated triboelectric nanogenerators and piezoelectric microsensors, Nano Energy 58 (2019) 612–623.

[69] F. Xi, Y. Pang, G. Liu, S. Wang, W. Li, C. Zhang, Z.L. Wang, Self-powered intelligent buoy system by water wave energy for sustainable and autonomous wireless sensing and data transmission, Nano Energy 61 (2019) 1–9.

[70] H. Wang, H. Wu, D. Hasan, T. He, Q. Shi, C. Lee, Self-powered dual-mode amenity sensor based on the water-air triboelectric nanogenerator, ACS Nano 11 (2017) 10337–10346.

[71] J. Chen, W. Xuan, P. Zhao, U. Farooq, P. Ding, W. Yin, H. Jin, X. Wang, Y. Fu, S. Dong, Triboelectric effect based instantaneous self-powered wireless sensing with self-determined identity, Nano Energy 51 (2018) 1–9.

[72] S. Wang, X. Mu, Y. Yang, C. Sun, A.Y. Gu, Z.L. Wang, Flow driven triboelectric generator for directly powering a wireless sensor node, Adv. Mater. 27 (2015) 240–248.

[73] K.-W. Lim, M. Peddigari, C.H. Park, H.Y. Lee, Y. Min, J.-W. Kim, C.-W. Ahn, J.-J. Choi, B.-D. Hahn, J.-H. Choi, A high output magneto-mechano-triboelectric generator enabled by accelerated water-soluble nano-bullets for powering a wireless indoor positioning system, Energy Environ. Sci. 12 (2019) 666–674.

[74] B. Zhang, J. Chen, L. Jin, W. Deng, L. Zhang, H. Zhang, M. Zhu, W. Yang, Z. L. Wang, Rotating-disk-based hybridized electromagnetic–triboelectric nanogenerator for sustainably powering wireless traffic volume sensors, ACS Nano 10 (2016) 6241–6247.

[75] G. Cheng, Z.-H. Lin, L. Lin, Z.-l. Du, Z.L. Wang, Pulsed nanogenerator with huge instantaneous output power density, ACS Nano 7 (2013) 7383–7391.

[76] G. Cheng, L. Zheng, Z.H. Lin, J. Yang, Z. Du, Z.L. Wang, Multilayered electrode based triboelectric nanogenerators with managed output voltage and multifold enhanced charge transport, Adv. Energy Mater. 5 (2015) 1401452.

[77] J. Luo, L. Xu, W. Tang, T. Jiang, F.R. Fan, Y. Pang, L. Chen, Y. Zhang, Z.L. Wang, Direct current triboelectric nanogenerator realized by air breakdown induced ionized air channel, Adv. Energy Mater. 8 (2018) 1800889.

[78] G. Cheng, Z.H. Lin, Z. Du, Z.L. Wang, Increase output energy and operation frequency of a triboelectric nanogenerator by two grounded electrodes approach, Adv. Funct. Mater. 24 (2014) 2892–2898.

[79] H. Qin, G. Cheng, Y. Zi, G. Gu, B. Zhang, W. Shang, F. Yang, J. Yang, Z. Du, Z. L. Wang, High energy storage efficiency triboelectric nanogenerators with unidirectional switches and passive power management circuits, Adv. Funct. Mater. 28 (2018) 1805216.

[80] A. Ghaffarinejad, J.Y. Hasani, R. Hinchet, Y. Lu, H. Zhang, A. Karami, D. Galayko, S.-W. Kim, P. Basset, A conditioning circuit with exponential enhancement of output energy for triboelectric nanogenerator, Nano Energy 51 (2018) 173–184.

[81] X. Liang, T. Jiang, G. Liu, T. Xiao, L. Xu, W. Li, F. Xi, C. Zhang, Z.L. Wang, Triboelectric nanogenerator networks integrated with power management module for water wave energy harvesting, Adv. Funct. Mater. (2019) 1807241.

[82] H. Wang, J. Wang, T. He, Z. Li, C. Lee, Direct muscle stimulation using diode-amplified triboelectric nanogenerators (TENGs), Nano Energy 63 (2019), 103844.

[83] W. Yin, Y. Xie, J. Long, P. Zhao, J. Chen, J. Luo, X. Wang, S. Dong, A self-power-transmission and non-contact-reception keyboard based on a novel resonant triboelectric nanogenerator (R-TENG), Nano Energy 50 (2018) 16–24.

[84] Y. Zou, P. Tan, B. Shi, H. Ouyang, D. Jiang, Z. Liu, H. Li, M. Yu, C. Wang, X. Qu, A bionic stretchable nanogenerator for underwater sensing and energy harvesting, Nat. Commun. 10 (2019) 2695.
[85] Z.L. Wang, J. Chen, L. Lin, Progress in triboelectric nanogenerators as a new energy technology and self-powered sensors, Energy Environ. Sci. 8 (2015) 2250–2282.
[86] Z. Lin, J. Yang, X. Li, Y. Wu, W. Wei, J. Liu, J. Chen, J. Yang, Large-scale and washable smart textiles based on triboelectric nanogenerator arrays for self-powered sleeping monitoring, Adv. Funct. Mater. 28 (2018) 1704112.
[87] X. Pu, H. Guo, J. Chen, X. Wang, Y. Xi, C. Hu, Z.L. Wang, Eye motion triggered self-powered mechnosensational communication system using triboelectric nanogenerator, Sci. Adv. 3 (2017), e1700694.

Feng Wen Received her B.Eng. degree in the School of Mechanical and Electric Engineering at Soochow University, Suzhou, China, in 2017. She is now a Ph.D. student in the Department of Electrical and Computer Engineering, NUS. Her research interests are focused on energy harvesting and wearable sensors.

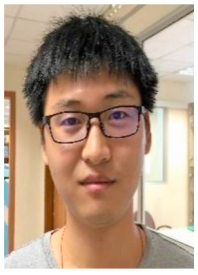

Hao Wang Received his B.Eng. degree in School of Optoelectronic Information from University of Electronic Science and Technology of China in 2010, and Ph.D. degree from the National University of Singapore in 2016. He is currently a Research Fellow of ECE, NUS. His research interests are focused on nanoneedle devices for transdermal drug delivery, flexible and wearable electronics, energy harvesting and electrical neural stimulations.

Tianyiyi He received her B.Eng. degree from the School of Microelectronics and Solid-state Electronics at the University of Electronic Science and Technology of China (UESTC), Chengdu, China, in 2016. She is now a Ph.D. candidate in the Department of Electrical and Computer Engineering, National University of Singapore. Her research interests include energy harvesters, triboelectric nanogenerator, thermoelectric energy harvester, and self-powered sensors.

Qiongfeng Shi received his B.Eng. degree from the Department of Electronic Engineering and Information Science, University of Science and Technology of China (USTC) in 2012 and received his Ph.D. degree from the Department of Electrical and Computer Engineering, National University of Singapore (NUS) in 2018. He is currently a Research Fellow in the Department of Electrical and Computer Engineering, National University of Singapore. His research interests include energy harvesters, triboelectric nanogenerators, self-powered sensors, and wearable/implantable electronics.

Zhongda Sun received his B.Eng. degree from the School of Electronic and Information at Soochow University, **Suzhou**, China, in 2018. After that he received his M.Sc degree from the Department of Electrical and Computer Engineering, NUS, in 2019. He is now a PhD student at the Department of Electrical and Computer Engineering, NUS. His research interests include self-powered wearable sensors and triboelectric nanogenerator.

Minglu Zhu Received his B.Bus. degree in Business Administration from the School of Business at State University of Bangladesh, Dhaka, Bangladesh, in 2010, and B.Sc. degree in Materials Science and Engineering from the School of Materials Science and Engineering at University of Illinois at Urbana-Champaign, Illinois, United States, in 2014. He is now a Ph.D. student at the Department of Electrical & Computer Engineering, NUS. His research interests focus mainly on MEMS based energy harvesters and self-powered sensors.

Zixuan Zhang received his B.Eng. degree from the School of Mechanical and Electrical Engineering at the University of Electronic Science and Technology of China (UESTC), Chengdu, China, in 2018. After that he received his M.Sc degree from Department of Electrical and Computer Engineering at National University of Singapore (NUS) in 2019. His research interests are focused on energy harvesters, self-powered sensors and triboelectric nanogenerator.

Zhiguang Cao received the B.Eng. degree from the School of Electrical Engineering, Nanjing Agricultural University, Nanjing, China, in 2016. He is now a M.Eng. candidate in the Suzhou Institute of Nano-tech and Nano-bionics Chinese **Academy** of Sciences. His research interests include signal processing, system integration and embedded systems.

Yanbing Dai received her B.Eng. degree from School of Electronic and Information Engineering at Soochow University, Suzhou, China, in 2018. She is now a M.Sc. candidate in Electronics and Communication Engineering, University of Science and Technology of China (USTC). Her research interests include flexible hybrid electronic circuit and flexible human-machine interaction system.

Ting Zhang is a Professor at Suzhou Institute of Nanotech and Nanobionics, Chinese Academy of Sciences. He received his B.S. (1999) and M.S. (2002) degree from Nankai University, and Ph. D. degree in chemical engineering at University of California, Riverside in 2007. His research mainly focuses on the development of smart materials, micro/nanosensing devices and smart microsystems for medical diagnostics, robotics, and environmental monitoring applications. He has published more than 60 peer-review papers in journals like Advanced Materials, Science Advances, Nano Letters, etc., and applied more than 30 patents.

Chengkuo Lee received his Ph.D. degree in Precision Engineering from The University of Tokyo in 1996. Currently, he is the **director** of Center for Intelligent Sensors and MEMS at National University of Singapore, Singapore. In 2001, he cofounded Asia Pacific Microsystems, Inc., where he was the Vice President. From 2006 to 2009, he was a Senior Member of the Technical Staff at the Institute of Microelectronics, A-STAR, Singapore. He has contributed to more than 300 peer-reviewed international journal articles.